

Supplementary Information for

Collective fluorescence enhancement in nanoparticle clusters

Siyang Wang,¹ Claudia Querner,¹ Tali Dadosh,¹ Catherine H. Crouch,² Dmitry S. Novikov³ and Marija Drndic^{1*}

¹*Department of Physics and Astronomy, University of Pennsylvania, Philadelphia, PA 19104, USA;*

²*Department of Physics and Astronomy, Swarthmore College, Swarthmore, PA 19081, USA;* ³*Center for Biomedical Imaging, New York University School of Medicine, New York, NY 10016, USA.*

**e-mails: drndic@physics.upenn.edu*

Table of contents

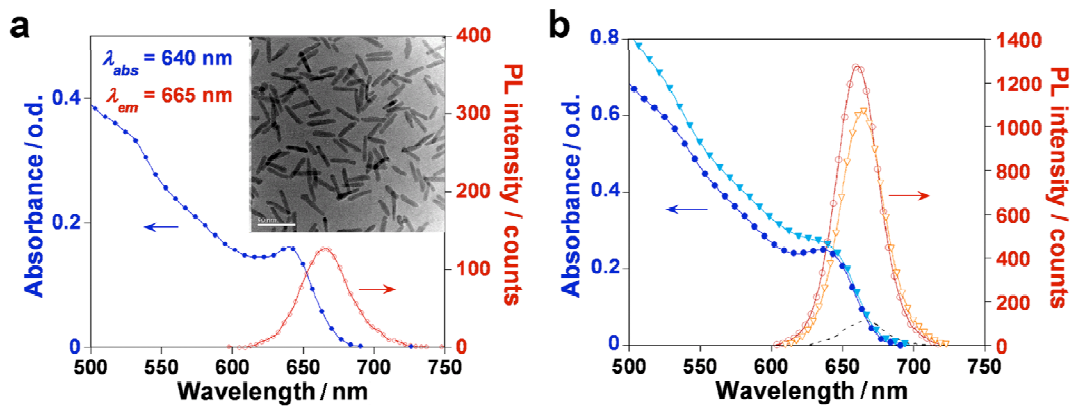
Supplementary Figures S1-S13

Supplementary Table S1

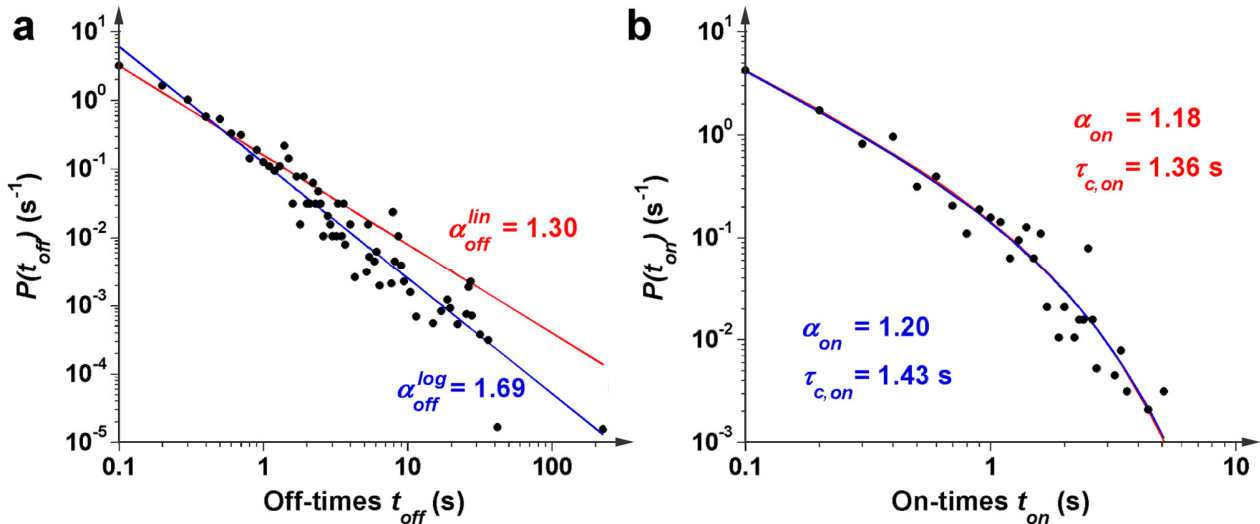
Supplementary Note 1

Supplementary Methods

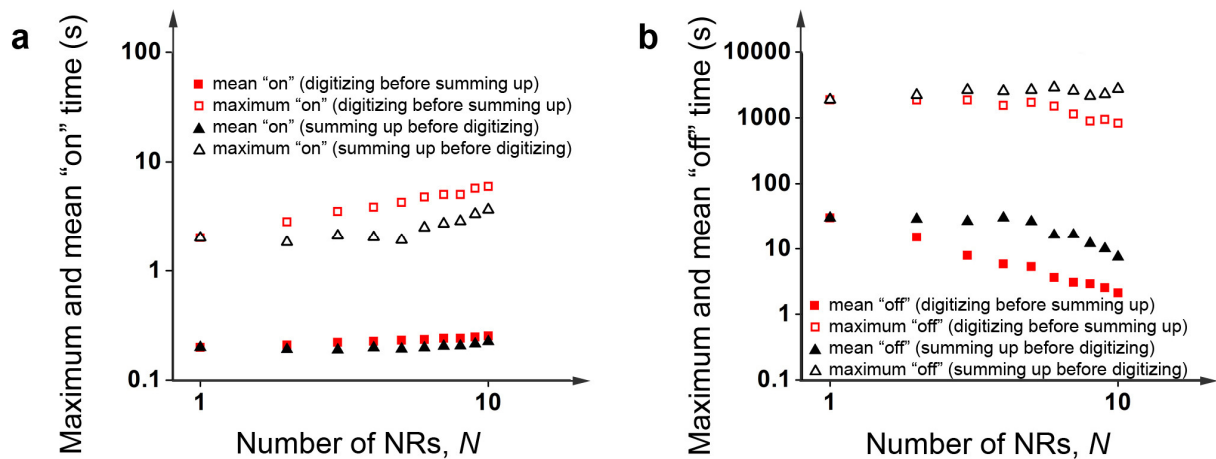
Supplementary References



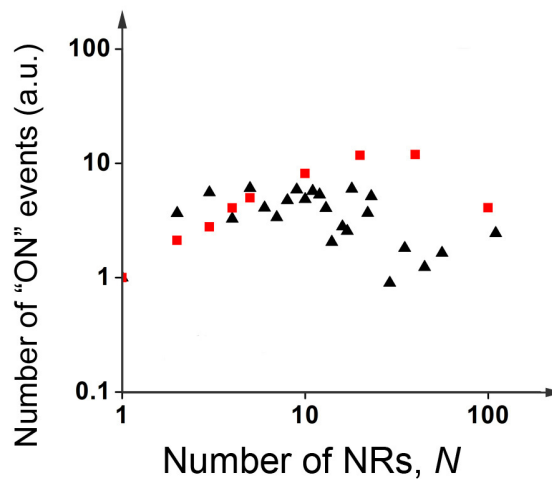
Supplementary Figure S1. nanorod synthesis and characterization **a**, Absorption and emission spectra of CdSe core NRs recorded in toluene. The inset shows a TEM image (the scale bar is 50 nm) of this sample. **b**, Absorption and emission spectra of CdSe/ZnSe core/shell NRs (circles, dark blue and red) and of CdSe/ZnSe/ZnS core/double shell NRs (triangles, light blue and orange). For comparison, the emission of the core NRs is indicated as dashed line. More details are in Supplementary Methods.



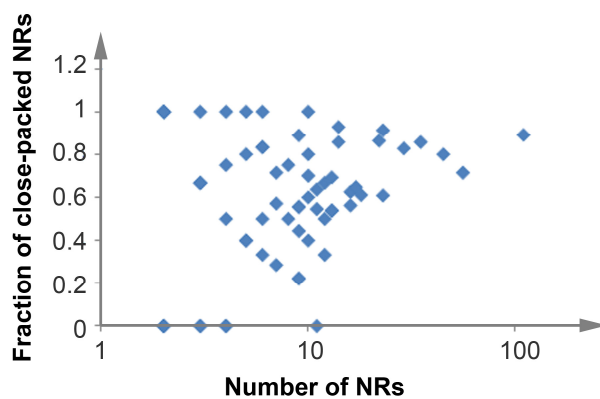
Supplementary Figure S2. Fitting methods for off- and on-time probability densities **a**, Off-time probability density of an individual NR, fitted by a power-law (red line, $\alpha_{off}^{lin} = 1.30$) or fitted by a line to the log-log data (blue line, $\alpha_{off}^{log} = 1.69$). **b**, On-time probability density of an individual NR, fitted by a truncated power law where both parameters are unconstrained (blue line, $\alpha_{on} = 1.20$, $\tau_{c,on} = 1.43$ s) and fitted by a sequential fitting method, where first α_{on} is determined by fitting the first four points, followed by the truncated power law fit (red line, $\alpha_{on} = 1.18$, $\tau_{c,on} = 1.36$ s). More details are in Supplementary Methods.



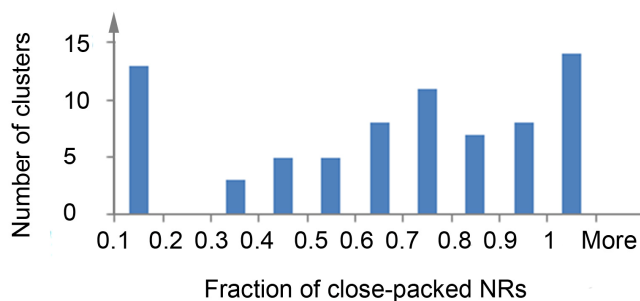
Supplementary Figure S3. Integration methods of fluorescence signals from independent NRs Scaling of **a.** mean and maximum on-times and **b.** mean and maximum off-times with the cluster size N using two methods of integrating independent single NRs, thresholding and digitizing before summing up (red squares) and summing up before thresholding and digitizing (black triangles). More details are in Supplementary Methods.



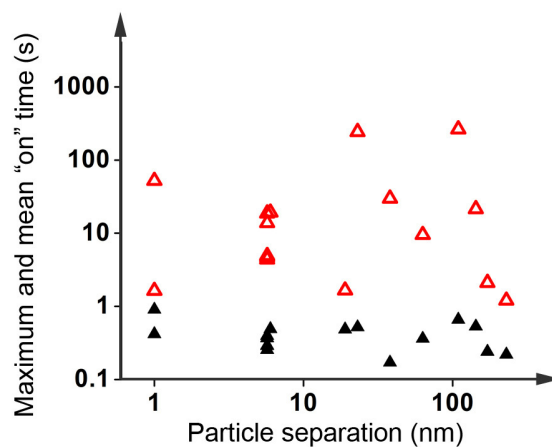
Supplementary Figure S4. The total number of "on" events The total number of "on" events vs. the cluster size N (black triangles) compared with data obtained from a Monte-Carlo simulation of N non-interacting particles (red squares). This number on the y-axis was normalized to the data of $N = 1$ to account for the different lengths of the movies in the Monte-Carlo simulation compared to the cluster data. It shows that the total number of "on" events decreases in clusters of N NRs compared to the collection of independent NRs, *i.e.*, fluorescence time traces of clusters consist of a relatively smaller number of on-events that are on average longer, as described in the main article.



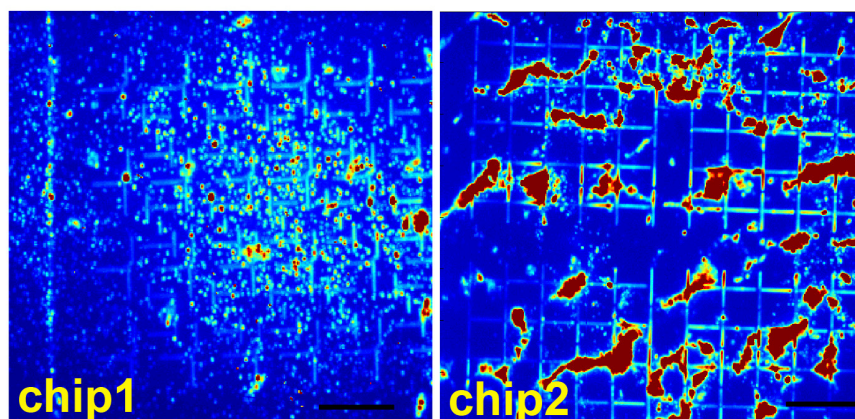
Supplementary Figure S5. Fraction of close-packed NRs vs number of NRs of 74 clusters. Some of the data points are overlapping, e.g. there are two $N=9$ clusters which are having a fraction of 0.56. More details are in Supplementary Note 1.



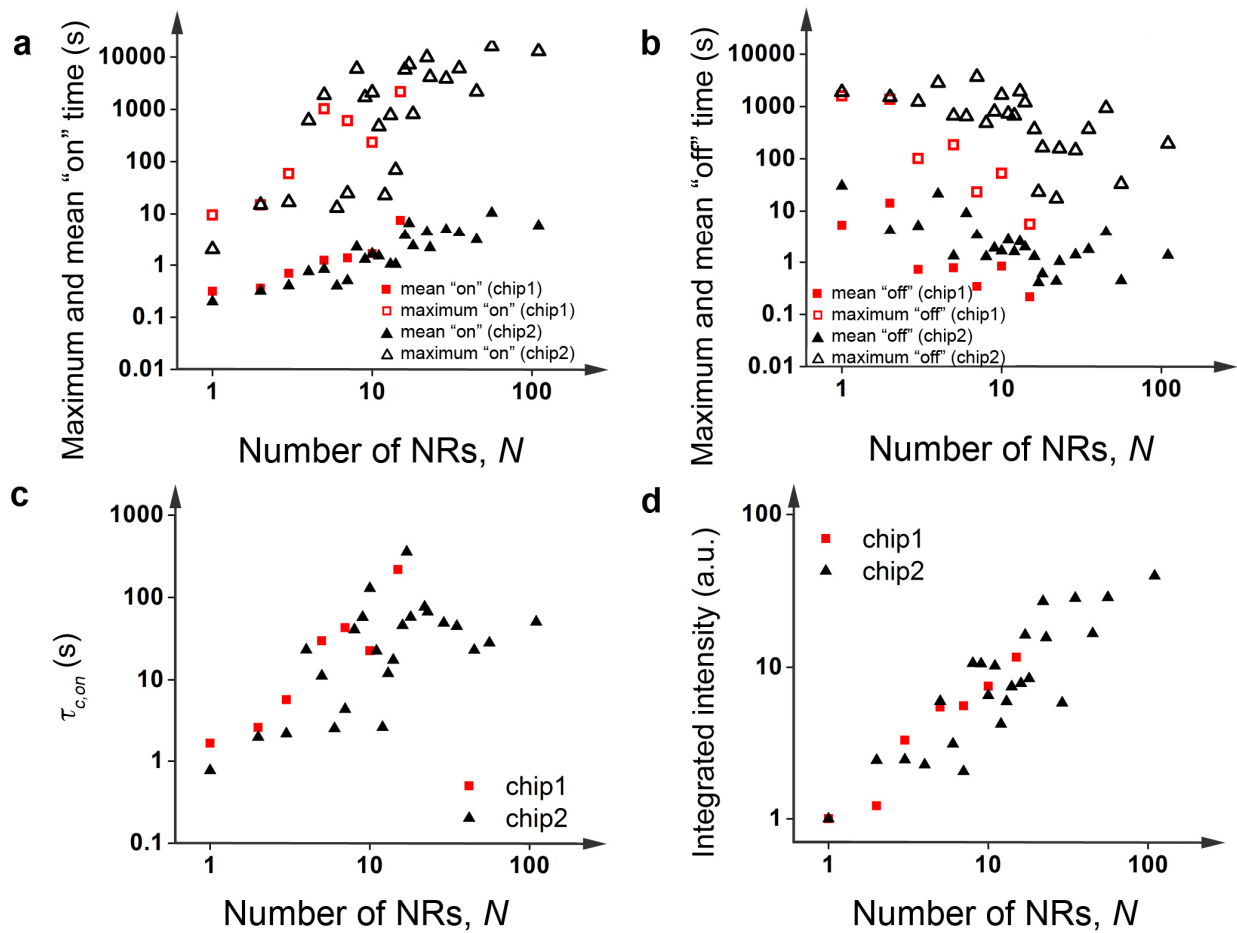
Supplementary Figure S6. Histogram of the fraction of close-packed NRs in clusters. More details are in Supplementary Note 1.



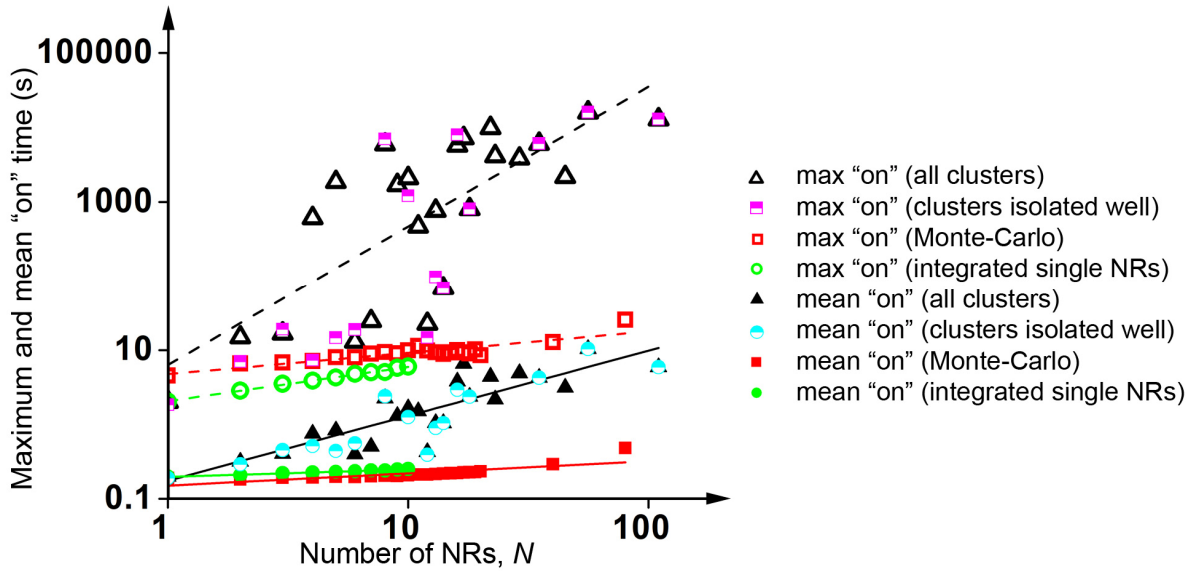
Supplementary Figure S7. Inter-particle distance dependence of on-times Mean and maximum on-time vs. inter-particle separation of cluster with $N = 2$.



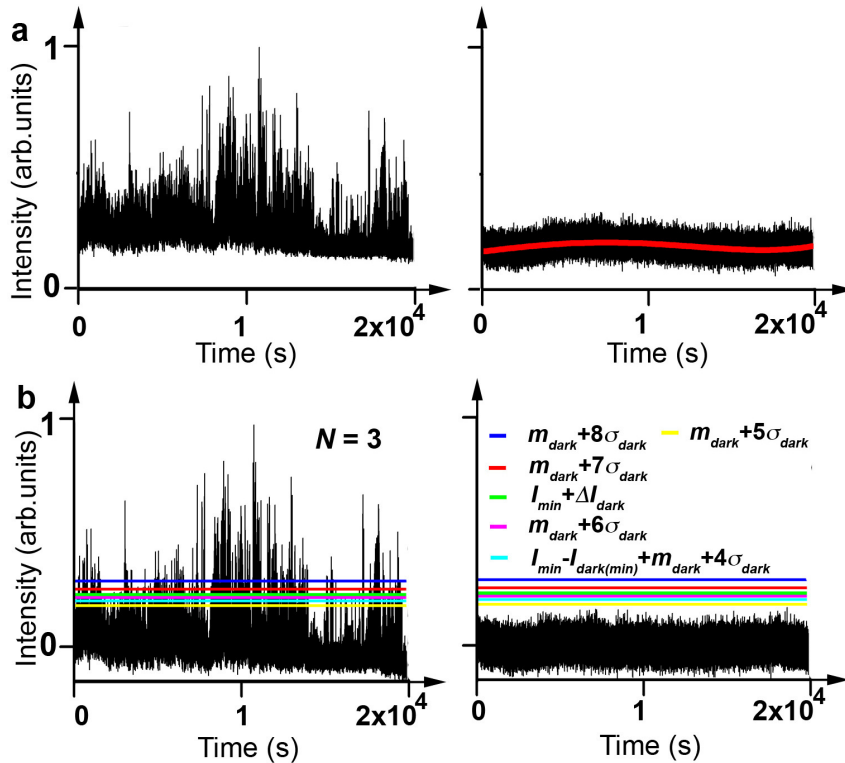
Supplementary Figure S8. Fluorescence micrographs of two silicon nitride chips measured independently. The scale bar is 10 μm . We made independent measurements several months apart, under the same experimental conditions on samples prepared by spin-casting solutions of the same NRs on two identically prepared silicon nitride chips. Chip 2 was prepared with a higher concentration NR solution in order to produce more clusters. The larger red areas correspond to extended regions in which individual clusters were not optically resolvable. We only analyzed data from clusters optically resolvable from their neighbours, as shown in Figure 7.



Supplementary Figure S9. Comparison of the results from two independent measurements **a**, Scaling of mean and maximum on-times with the cluster size N from chip1 (open and solid red squares) compared with on-times obtained from chip2 (open and solid black triangles). Chip 1 and 2 are the chips shown in Supplementary Figure S8. **b**, Scaling of mean and maximum off-times with the cluster size N from chip1 (open and solid red squares) compared with off-times obtained from chip2 (open and solid black triangles). **c**, Scaling of $\tau_{c,on}$ with the cluster size N measured on chip1 (red squares) compared with data obtained from chip2 (black triangles). **d**, Scaling of the integrated intensity with the cluster size N measured on chip1 (red squares) compared with data obtained from chip2 (black triangles).



Supplementary Figure S10. Effect of segmenting methods on on-times. Scaling of mean and maximum on-times with the cluster size N from 42 completely isolated bright spots (half-solid pink squares and cyan circles) compared with on-times obtained from all 120 bright spots in Figure 4c (open and solid black triangles), integrating signals from N isolated NRs located on the same chip (Figure 4c, open and solid green circles) and with results from a Monte-Carlo simulation of N non-interacting particles (Figure 4c, open and solid red squares). More details are in Methods in the main text.



Supplementary Figure S11. Threshold analysis of a cluster with $N=3$ **a**, Intensity trajectory of the cluster with $N = 3$ in Figure 8a and an intensity trajectory of a nearby dark region with a polynomial fit. **b**, Fluorescence intensity vs. time, $I(t)$, after background subtraction from the same cluster and a nearby dark region. Different lines (color) are the different threshold levels defined as $m_{dark} + 8\sigma_{dark}$, $m_{dark} + 7\sigma_{dark}$, $I_{min} + \Delta I_{dark}$, $m_{dark} + 6\sigma_{dark}$, $I_{min} - I_{dark(min)} + m_{dark} + 4\sigma_{dark}$, and $m_{dark} + 5\sigma_{dark}$ from high to low, where m_{dark} , σ_{dark} , ΔI_{dark} and $I_{dark(min)}$ are the

Fraction of close-packed NRs	0	0.67	0.5	0	0.75	1	0	0	1	0.8	0.4	0.4	0.5	0.83	1	0.83	0.33	0.71
Number of NRs	7	7	8	8	9	9	9	9	9	9	10	10	10	10	10	11	11	11
Fraction of close-packed NRs	0.57	0.29	0.5	0.75	0.22	0.44	0.56	0.22	0.56	0.89	0.7	0.6	0.8	0.4	1	0	0.55	0.64
Number of NRs	12	12	12	13	13	13	14	14	16	16	17	18	22	23	23	29	35	45
Fraction of close-packed NRs	0.5	0.33	0.67	0.54	0.54	0.69	0.86	0.93	0.56	0.63	0.65	0.61	0.86	0.91	0.61	0.83	0.86	0.8
Number of NRs	56	110																
Fraction of close-packed NRs	0.71	0.89																

Supplementary Note 1

Estimates of electric field-induced exciton rearrangement and field-driven coordinated trapping/detrapping

a) Field-induced exciton rearrangement: A charge moving a distance a from a NR core to a neighboring trap would cause a change $E = \text{const} \cdot ea/\epsilon r^3$ in the electric field at a distance $r \gg a$ equivalent to a field from a dipole with the dipole moment ea . Even in the case of $r \sim a$, which applies to NRs very close to each other, this formula would still yield a correct order-of-magnitude estimate. Here ϵ is the effective dielectric constant of the environment, $\epsilon = (\epsilon_{\text{substr}} + 1)/2 \approx 4$, where $\epsilon_{\text{substr}} = 7.5$ for SiN according to Ref 37. The prefactor ‘const’ in the expression for the magnitude of E depends on the angle θ between the direction \mathbf{a} of the hop and the given direction \mathbf{r} , as $(1 + 3\cos^2\theta)^{1/2}$, which varies between 1 and 2, as well as on the further details of the dielectric environment (the depolarization factors, etc), see e.g. Ref. 38.

As a result, using $e^2/(1 \text{ nm}) = 1.44 \text{ eV}$, we obtain for the electric field $E \sim (1 \dots 2) \cdot 1.44 \cdot (a/r^3)/\epsilon \text{ V/nm}$, where a and r are in nm. Note that $1 \text{ V/nm} = 10 \text{ MV/cm}$; with the hop distance $a = 4 \text{ nm}$ compatible with the wave function size within a NR, and $r = 8 \text{ nm}$ the distance to a neighbouring NR, find $E \sim 11 \dots 22 \text{ mV/nm} = 110 \dots 220 \text{ kV/cm}$ applied (unscreened) field depending on the direction, which, according to the measurements of Rothenberg et al,³⁹ could cause switching of a neighbouring NR at a distance r .

b) Field-driven coordinated trapping/detrapping: Now let us consider a *dynamic* effect of a sudden change in the electric field on an electron trapped in a vicinity of a given NR, due to switching off of a neighboring NR caused by the hop of its electron onto the corresponding nearby trap. This sudden field change can potentially cause the release (a “shake-up”) of the trapped electron back on a given NR, thereby switching it on.

While any precise calculation would require detailed information about the character of a trapping potential, we may still make some order-of-magnitude estimates. First, assume a trapped electron in a ground state of an approximately harmonic oscillator potential with the oscillator frequency (potential curvature) ω_0 . Under a sudden change of an electric field E at the position of an oscillator, the probability P_k to get excited to the k^{th} oscillator level is given by the Poissonian distribution $P_k = (\lambda^k/k!) \cdot \exp(-\lambda)$, where $\lambda = (eE)^2/(2m\hbar\omega_0^3)$, see Ref. 40. As a realistic trap potential likely has only one or a few bound states, one can qualitatively assume that the shake-up occurs with a notable probability

if the corresponding oscillator shake-up parameter $\lambda \sim 1$ (*i.e.* not small). For an estimate, we would also assume that the trap binding energy is of the order of oscillator energy spacing, $E_{\text{trap}} \sim \hbar\omega_0$, consistent with the above assumption of only a few eigenlevels in a trap. From the condition $\lambda \sim 1$ we obtain the maximal depth E_{trap} of the trap that could be depleted by the shake-up over a distance r : $E_{\text{trap}} \sim (eE(r))^{2/3} (\hbar^2/2m)^{1/3}$. Since $\hbar^2/(2m) = 38 \text{ meV}\cdot\text{nm}^2$ [m is the electron mass; the effective mass may be notably smaller depending on where the trap is located which would increase E_{trap}], and $eE \sim 10 \text{ meV/nm}$ for r and a as above (depending on the effective dielectric constant and orientation), obtain $E_{\text{trap}} \sim 10\text{-}100 \text{ meV}$, which is compatible with energies of shallow traps. When $r \sim 1 \text{ nm}$ rather than 10 nm , *i.e.* NRs are very close, E_{trap} can exceed 0.1 eV , covering a wider portion of the trap energies.

Overall, we expect the dynamic field-driven effect acts on a similar distance scale as direct charge tunneling ($\sim 2 \text{ nm}$). The short-range character of both effects is fundamentally due to the fact that both the dipole field (in the first case) and its square entering the shake-up matrix element (in the second case), decrease faster than $1/r^d$, thereby being effectively short-ranged in the $d=2$ -dimensional geometry of our clusters. Our estimates indicate that static field-driven distortion may be somewhat longer ranged (up to $\sim 8 \text{ nm}$).

Fraction of close-packed NRs within clusters

We analyzed the TEM images of the clusters to determine the fraction of close-packed NRs in each. Supplementary Figure S5 shows the fraction of close-packed NRs *vs* the number of NRs in the cluster for 74 clusters. There is a broad distribution of the fraction of close-packed NRs; nearly all clusters have at least a few close-packed NRs (60 out of 74 clusters). Some of the data points are overlapping, *e.g.* two $N=9$ clusters each have the same fraction (0.56) close-packed. Supplementary Figure S6 shows the histogram of the fraction of close-packed NRs of the 74 clusters. Most clusters have between 50% and 80% of NRs close-packed with at least one neighbor. However, almost none of the clusters for $N > 2$ are fully close-packed. We also show the fraction of close-packed NRs in Table S1 for reference.

Supplementary Methods

Experimental details of nanorod synthesis and characterization

CdSe/ZnSe/ZnS core/double shell semiconductor nanorods (NRs) are prepared in a two-step procedure.

First, CdSe core NRs having a diameter of 5.8 nm and a length of 34 nm are synthesized using a multiple injection method.⁴¹ In detail, 45.1 mg of cadmium oxide (CdO, Aldrich, 99%) have been placed with 140.9 mg of decylphosphonic acid (DPA, Alfa Aesar, 99%) and 5.5 g of tri n-octylphosphine oxide (TOPO, Aldrich, 90%) under nitrogen atmosphere and were heated to 300°C for approximately 2 hours until the initially red-brown suspension turned colorless. Independently, a solution of 563 mg of selenium powder (Se, Aldrich, 99.99%) was dissolved in 7 mL of tri n-octylphosphine (TOP, Aldrich, 99%). The TOPSe solution was injected slowly into the Cd-precursor solution in aliquots of 0.1 mL (5 times, 2 minute waiting between each injection), 0.2 mL (5 times, every 3 minutes), and finally 0.4 mL (10 times, every 5 minutes). The initial injection temperature was

295°C, which was gradually reduced via 280°C (during the 0.2 mL injections) to 270°C (for the 0.4 mL injections). The reaction was stopped after 80 minutes by removing the heating source and the growth solution was allowed to cool to 60°C, when 20 mL of methanol were added to precipitate the NRs. After centrifugation and washing additionally with methanol (three times), the NRs were dispersed in toluene for optical characterization (Supplementary Figure S1a).

The absorption spectrum (USB-2000 spectrometer, Ocean Optics) is characterized by an excitonic peak at 640 nm. Concentration dependent absorption measurements allowed us to determine an absorption cross-section at 488 nm to be $4.22 \cdot 10^{-14} \text{ cm}^2$.⁶ The emission (USB-4000FL spectrometer, Ocean Optics, excitation: 470 nm LED, 35 μW) of these NRs is centered at 665 nm with a full-width at half maximum (FWHM) of 38 nm, i.e., this sample exhibits a Stokes shift of 15 nm. Comparing the area of the emission peak to the one of an aqueous solution of rhodamine 6G adjusted to an identical optical density at the excitation wavelength allows us to estimate a fluorescence quantum yield of 0.3%.

These NRs were further characterized by high-resolution transmission electron microscopy (HR-TEM, JEOL 2010F) after deposition on holey carbon grids from a dilute solution. From the TEM images (Supplementary Figure S1a inset) we determined a NR size of $\sim 5.8 \times 34 \text{ nm}$, meaning the aspect ratio is ~ 5.9 .

Subsequently, the CdSe core NRs were capped with a thin intermediate ZnSe shell and a thicker ZnS outer shell to prepare the CdSe/ZnSe/ZnS core/double shell system.⁴² In particular, $4.4 \cdot 10^{-9} \text{ mol}$ of the CdSe core rods have been mixed with 5.0 g of TOPO and 3 g of hexadecylamine (HDA, Aldrich, 90%). Solutions of 0.08 M TOPSe (6.4 mg Se in 1 mL TOP) and 50 mg of zinc stearate (ZnSt, Aldrich, 99%) in 1 mL of dioctylamine (DOA, Aldrich, 99%) are prepared and mixed together. These quantities should correspond to the formation of 1 monolayer (ML) of ZnSe. At 225°C, this solution is slowly injected over a period of 10 min. The reaction mixture is allowed to stir for another 15 minutes.

To half to the above reaction mixture, still at 225°C, a total of 7 mg bis-(trimethylsilyl)-sulfur ((TMS)₂S, Aldrich, 99%) and 125 mg of ZnSt in 6 mL DOA are injected over a period of 30 minutes. These quantities should lead to the growth of 5 ML of ZnS. The reaction mixture is allowed to continue stirring for 10 minutes after complete injection and finally to cool. Purification is carried out by precipitating the sample in methanol.

The absorption and emission spectra of the core/shell(s) systems are summarized in Supplementary Figure S1b. The absorption of all three samples is very similar with the main difference being an increase in absorption at higher energies (*i.e.*, at smaller wavelengths) with increasing shell thickness. The width of the emission peak remains unchanged upon shell growth and is slightly red-shifted (with increasing shell(s) thickness) compared to the core NRs. The fluorescence quantum yield increases significantly during the shell growth: from 0.3% for the CdSe core sample to 1.7% for the CdSe/ZnSe core/shell NRs and 1.6% for the CdSe/ZnSe/ZnS core/double shell NRs. These values are obtained for the extensively purified samples. For samples taken at intermediate stages of the shell growth, recorded in solutions containing still excess surface ligands such as HDA or DOA, fluorescence quantum yields of up to 14% for the core/shell NRs and 6.1% in the case of the core/double shell NRs have been measured.

Fitting methods of probability densities for on- and off-times

From the intensity time-traces, $I(t)$, of the fluorescent segments, we determined the probability densities for off- and on-events of duration t_{off} and t_{on} , respectively, using a weighted method to estimate the true probability of rare events.¹²

$$P(t_{off(on)}) = \frac{N(t_{off(on)})}{N_{off(on)}^{total}} \cdot \frac{1}{\Delta t_{off(on)}^{average}} \quad \text{with} \quad \Delta t_{off(on)}^{average} = \frac{a+b}{2} \quad \text{Eq. S1}$$

where $N(t_{off(on)})$ is the number of off (on) events of duration $t_{off(on)}$, $N_{off(on)}^{total}$ is the total number off (on) events, observed from that fluorescent segment, and $\Delta t_{off(on)}^{average}$ is related to the duration of the measurement frames. In the case of common event durations, a and b (time differences to the next longest and next shortest observed event) equal this frame duration and consequently $\Delta t_{off(on)}^{average} = 100$ ms. However, in the case of rare events, a or b exceeds 100 ms and $\Delta t_{off(on)}^{average}$ increases.

In our previous paper,⁶ we discussed how different fitting approaches influence the off-time power law exponents.

The probability densities are commonly plotted on a \log_{10} - \log_{10} scale as they largely follow a power law behavior. However, there is a more or less pronounced deviation from that behavior at long times. When fitting the data on a linear scale with a power law, the short events dominate in the fitting. The power law exponent ~ 1.3 (Supplementary Figure S2a) is relatively robust with respect to changes of samples, environment or laser intensity. However, a linear fit to the \log_{10} - \log_{10} plot accounts better for the long time data, leading to an increase in the exponent, $\alpha_{off}^{\log} \sim 1.7$, in the case of individual NRs.

The on-time probability densities deviate from the power law and are described by a “truncated power law”, the product of a power law and an exponential,

$$P(t_{on}) \propto t_{on}^{-\alpha_{on}} e^{-t_{on}/\tau_{c,on}}, \quad \text{Eq. S2}$$

where the truncation time, $\tau_{c,on}$, describes the transition between the two regimes. We previously used a fitting method where both the on-time exponent, α_{on} , and the truncation time, $\tau_{c,on}$, were left unconstrained.⁶ However, a two-step fitting method, where first, α_{on} is determined by fitting a line to the log of the data (*i.e.*, for on-times, $t_{on} < 0.5$ s) and second, where $\tau_{c,on}$ is determined while keeping α_{on} constant, was found to be more appropriate: the fitting parameters show higher consistency within one sample, and the associated errors are smaller. Supplementary Figure S2b compares the two fitting methods for the on-time probability density of an individual NR. For this particular NR trace, both fitting methods yield consistent results. However, in many cases, the first method underestimates the truncation time.

Integration of fluorescence signals from independent NRs and Monte-Carlo simulation

We compare the mean and maximum on-times of the integrated N independent single NRs to those of clusters with N NRs on the same chip. To compute the integrated data, two distinct approaches were used: In the first approach (“digitizing before summing”), we add trajectories digitized to be 0 or 1 by a threshold of N single NRs selected randomly from 14 single NRs found on the chip. We then determine the “on” events by setting a threshold of 0.5. In order to maximize the sampling size, we repeat a random selection and data analysis 30 times for $N = 1-10$ and take the average. In the second approach, (“summing before digitizing,”) we sum up the raw trajectories prior to background subtraction and digitization. We subsequently subtract the appropriate polynomial fit to the background and a threshold determined from the integrated background signal.

Next, we compare the maximum and mean on- and off-times using the two methods. Supplementary Figure S3a shows that the mean on-times of the two methods agree well, while the maximum on-times are smaller using the second method (black open triangles). In Supplementary Figure S3b, both mean and maximum off-times using the second method (black triangles) are larger than those results from the first method (red squares). The reason could be that the threshold in the second method was determined the same way as described in **Methods** in the main text, and it was elevated up too high due to the integration of background signals so that we lost some signals which should be considered “on”, which shortened the on-times and extended the off-times. The on-times from both methods are substantially lower than those of clusters data (Figure 4c shows on-times from the first method) and both support the conclusion in the main paper.

We do the Monte-Carlo simulation for a single NR by generating successive “on” and an “off” intervals according to the probability density function of the form of Eq. 1 in the main article for on- and off-times, respectively. We set $\tau_{c,on} = 1$ s, $\tau_{c,off} = 1000$ s, and $\alpha_{on} = \alpha_{off} = 1.5$, and assign 1 and 0 to “on” and “off” states correspondingly. For N independent NRs, we generate the single trajectories independently as described above, add them to form a net signal, and then digitize the result by assigning 1 for any time interval where the net signal is nonzero, and 0 otherwise.

Supplementary References

37. SiliconFarEast.com <http://www.siliconfareast.com/sio2si3n4.htm> 2004
38. Kovalev, D. *et al* Porous Si anisotropy from photoluminescence polarization. *Appl. Phys. Lett.* 67, 1585-1587 (1995).
39. Rothenberg, E., Kazes, M., Shaviv, E. and Banin U. Electric Field Induced Switching of the Fluorescence of Single Semiconductor Quantum Rods. *Nano Lett.* 5, 1581–1586 (2005).
40. L. D. Landau and E. M. Lifshitz, Quantum Mechanics (Non-Relativistic Theory), Third Edition: Volume 3, Sec. 41, Butterworth-Heinemann, Oxford (2003).
41. Shieh, F., Saunders, A. E. & Korgel, B. A. General shape control of colloidal CdS, CdSe, CdTe quantum rods and quantum rod heterostructures. *J. Phys. Chem. B* **109**, 8538-8542 (2005).
42. Reiss, P., Carayon, S., Bleuse, J. & Pron, A. Low polydispersity core/shell nanocrystals of CdSe/ZnSe and CdSe/ZnSe/ZnS type: preparation and optical studies. *Synth. Met.* **139**, 649-652 (2003).